Al0.2Ga0.8As X-ray photodiodes for X-ray spectroscopy

Article (Published Version)

Nuclear Instruments and Methods in Physics Research A 840 (2016) 168–173

Contents lists available at ScienceDirect

Nuclear Instruments and Methods in Physics Research A

journal homepage: www.elsevier.com/locate/nima

$Al_{0.2}Ga_{0.8}As$ X-ray photodiodes for X-ray spectroscopy

M.D.C. Whitaker*, G. Lioliou, S. Butera, A.M. Barnett

Semiconductor Materials and Devices Laboratory, Sch. of Engineering and Informatics, University of Sussex, Falmer, Brighton BN1 9QT, UK

ARTICLE INFO

Keywords:
X-ray detector
Photodiode
Spectroscopy

ABSTRACT

Three custom-made $Al_{0.2}Ga_{0.8}As$ p-i-n mesa X-ray photodiodes (200 μm diameter, 3 μm i layer) were electrically characterised and investigated for their response to illumination with soft X-rays from an ^{55}Fe radioisotope X-ray source (Mn Kα = 5.9 keV; Mn Kβ = 6.49 keV). The AlGaAs photodiodes were shown to be suitable for photon counting X-ray spectroscopy at room temperature. When coupled to a custom-made low-noise charge-sensitive preamplifier, a mean energy resolution (as quantified by the full width at half maximum of the 5.9 keV photopeak) of 1.24 keV was measured at room temperature. Parameters such as the depletion width (1.92 μm at 10 V), charge trapping noise (61.7 e^- rms ENC at 5 V, negligible at 10 V) and the electronic noise components (known dielectric noise (63.4 e^- rms), series white noise (27.7 e^- rms), parallel white noise (9.5 e^- rms) and $1/f$ series noise (2.2 e^- rms) at 10 V reverse bias) affecting the achieved energy resolution were computed. The estimated charge trapping noise and mean energy resolution were compared to similar materials (e.g. $Al_{0.8}Ga_{0.2}As$) previously reported, and discussed. These results are the first demonstration of photon counting X-ray spectroscopy with $Al_{0.2}Ga_{0.8}As$ reported to date.

1. Introduction

Since the first reported detection of X-rays with AlGaAs [1], the material has received increased attention as a promising alternative for X-ray [1–3] and beta particle [4,5] detection at room temperature and above. Results have been reported for a number of different Al fractions, but for X-ray spectroscopy, most work has concentrated on $Al_{0.8}Ga_{0.2}As$ for high temperature devices due to its wide bandgap (2.09 eV [6]). Compared to narrow bandgap materials, wide bandgap detectors can possess superior resolutions at high temperature (» 20 °C) due to lower thermally induced leakage currents [7] and thus lower parallel white noise [8]. This presents the possibility of reducing cooling requirements for X-ray detectors, with subsequent reduction of mass, volume, power requirements and hence, cost of the instrument; these improvements are important for applications including X-ray fluorescence spectroscopy for future space missions subjected to high temperature and intense radiation conditions, as well as terrestrial applications in industrial instrumentation.

Despite $Al_{0.8}Ga_{0.2}As$ having been subject to extensive study, depending on the operating environment, lower Al fractions of $Al_xGa_{1-x}As$ could be more beneficial; varying the Al fraction adjusts the material's bandgap, where a reduction in Al fraction reduces the bandgap. Thus, for more modestly elevated temperatures, $Al_{0.2}Ga_{0.8}As$ may provide a better solution than $Al_{0.8}Ga_{0.2}As$. This presumption is also based on the bandgap of $Al_{0.2}Ga_{0.8}As$ (1.67 eV [9]) being close to the optimal for a room temperature X-ray detector (1.5 eV [10,11]). In addition, the electron hole pair creation energy of $Al_{0.2}Ga_{0.8}As$ is likely to be lower than those for higher Al fraction $Al_xGa_{1-x}As$ (e.g. 5.1 eV for $Al_{0.8}Ga_{0.2}As$ at 294 K [12,13]), leading to an improved Fano limited resolution for $Al_{0.2}Ga_{0.8}As$ [13]. A reduction in Al fraction also leads to a larger X-ray linear attenuation coefficient (e.g. 787.8 cm^{-1} for $Al_{0.2}Ga_{0.8}As$ c.f. 638.8 cm^{-1} for $Al_{0.8}Ga_{0.2}As$, at 5.9 keV). That is to say, more photons are absorbed and scattered within the detecting material due to the increased material density, whereby GaAs possesses a greater density (5.32 g cm^{-3}) [14] in comparison to Al (2.69 g cm^{-3}) [14].

Furthermore, previous work on $Al_{0.8}Ga_{0.2}As$ for photon counting X-ray spectroscopy detectors has focused on thin i layers, e.g. 1 μm [4,15] and 1.7 μm [2]. This is due to the lattice mismatch between $Al_{0.8}Ga_{0.2}As$ and GaAs (the substrate material typically used for AlGaAs growth) which leads to relaxation when the wafer is cooled from growth temperatures. Whilst virtual substrate technology, in which graded Al fraction AlGaAs is grown on a GaAs substrate to provide a virtual $Al_{0.8}Ga_{0.2}As$ substrate, may enable thick, high quality $Al_{0.8}Ga_{0.2}As$ epilayers to be produced, comparatively thicker $Al_{0.2}Ga_{0.8}As$ layers can be grown on a commercial GaAs substrate directly.

Here, results characterising three prototype $Al_{0.2}Ga_{0.8}As$ X-ray p-i-n mesa photodiodes (200 μm diameter, 3 μm i layer) are presented. The devices were randomly selected from those grown and fabricated to

* Corresponding author.
E-mail address: M.Whitaker@sussex.ac.uk (M.D.C. Whitaker).

http://dx.doi.org/10.1016/j.nima.2016.10.017
Received 27 June 2016; Received in revised form 6 October 2016; Accepted 6 October 2016
Available online 07 October 2016

the Authors' specifications at the EPSRC National Centre for III-V Technologies, Sheffield, UK.

2. Diode design

$Al_{0.2}Ga_{0.8}As$ p-i-n layers topped by a thin GaAs buffer layer were grown by metalorganic chemical vapour phase epitaxy (MOVPE) on a commercial 2 in. GaAs n^+ substrate. The layer details are summarised in Table 1. Circular mesa structures (200 μm diameter) were formed using 1:1:1 H_3PO_4:H_2O_2:H_2O solution followed by 10 s in 1:8:80 H_2SO_4:H_2O_2:H_2O solution. An Ohmic contact consisting of 20 nm InGe and 200 nm Au was evaporated onto the rear substrate, and an Ohmic top contact of 20 nm Ti and 200 nm Au was evaporated onto the p^+ side of the mesa devices; the top contact covered 45% of each diode's face. The devices were unpassivated.

Table 1
Layer details of the $Al_{0.2}Ga_{0.8}As$ wafer.

Layer	Material	Thickness (μm)	Dopant	Dopant type	Doping density (cm^{-3})
1	GaAs	0.01	Be	P	1×10^{19}
2	$Al_{0.2}Ga_{0.8}As$	0.5	Be	P	2×10^{18}
3	$Al_{0.2}Ga_{0.8}As$	3	Undoped		
4	$Al_{0.2}Ga_{0.8}As$ Substrate: GaAs	1	Si	N	2×10^{18}

3. Experiment results

3.1. Capacitance as a function of applied reverse bias

Capacitance as a function of applied reverse bias was measured for each $Al_{0.2}Ga_{0.8}As$ p-i-n photodiode, D1–D3, at a temperature of 22 °C, using an HP 4275A LCR Meter (signal magnitude 60 mV rms; frequency 1 MHz) and an HP 16065A EXT Voltage Bias Fixture. A Keithley 6487 picoammeter/voltage source was used to bias the detectors. The measured capacitances were consistent across all devices. Fig. 1 presents the capacitance as a function of applied reverse bias for one representative diode (D1); comparable results were found for the other devices. As the devices were measured after packaging, the capacitance of the package was removed by measuring the capacitance of four empty connections on the same package (0.65 pF ± 0.04 pF rms) and deducting this from the total capacitance obtained for each diode. The capacitance of the bond wire of each detector was not individually separated from the packaging capacitance, but the subsequent analysis suggests that the bond wire capacitances were insignificant compared with the other system capacitances. The capacitances of the devices at 10 V and 30 V were 1.81 pF ± 0.02 pF and 1.14 pF ± 0.02 pF, respectively.

From the measured depletion layer capacitance $C_{DL}(V_R)$, the depletion width of the diodes as a function of applied reverse bias $W(V_R)$ was calculated using,

$$C_{DL}(V_R) = \frac{\varepsilon_0 \varepsilon A}{W(V_R)}, \quad (1)$$

where ε_0 is the permittivity of free space, ε is relative permittivity of the material (12.332 for $Al_{0.2}Ga_{0.8}As$ [16]), and A is the area of the device [17]. From the measured depletion layer capacitance of the $Al_{0.2}Ga_{0.8}As$ photodiode D1 shown in Fig. 1, depletion widths of 1.92 μm ± 0.05 μm and 3.06 μm ± 0.12 μm were calculated at reverse biases of 10 V and 30 V, respectively. Fig. 2 shows the calculated depletion width as a function of applied reverse bias for D1 $Al_{0.2}Ga_{0.8}As$. Beyond 30 V, the measured depletion layer capacitance and consequently the depletion width, remained constant, suggesting that the diodes were fully depleted at a reverse bias of 30 V. The carrier concentration in the i layer was determined from capacitance measurements to be 4×10^{15} cm^{-3}. Further refinement and optimisation of the growth process may improve (reduce) the unintentional doping concentration in the i layer, which may lead to performance improvements.

The implied detection efficiency of the $Al_{0.2}Ga_{0.8}As$ diodes when reverse biased at 10 V (mean depletion width of 1.90 μm ± 0.05 μm) and 30 V (mean depletion width of 3.02 μm ± 0.12 μm) as functions of energy are shown in Fig. 3. The detection efficiencies of two previously

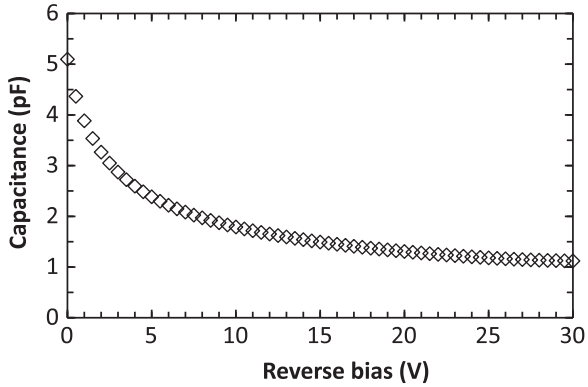

Fig. 1. Measured capacitance as a function of applied reverse bias for one representative $Al_{0.2}Ga_{0.8}As$ X-ray p-i-n mesa photodiode, D1, at room temperature. Comparable results were obtained for the other devices.

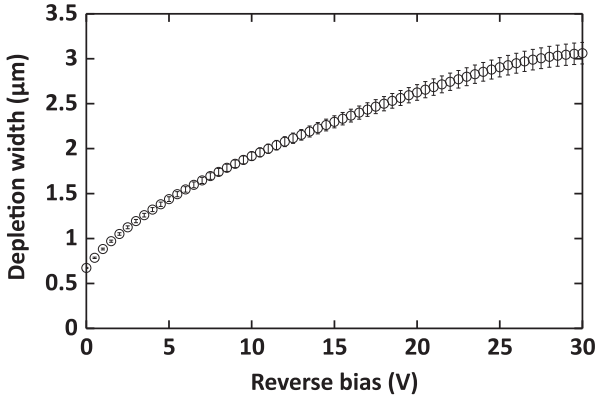

Fig. 2. Calculated depletion width as a function of applied reverse bias for D1 $Al_{0.2}Ga_{0.8}As$ (200 μm diameter, 3 μm i layer). Comparable results were obtained for the other devices.

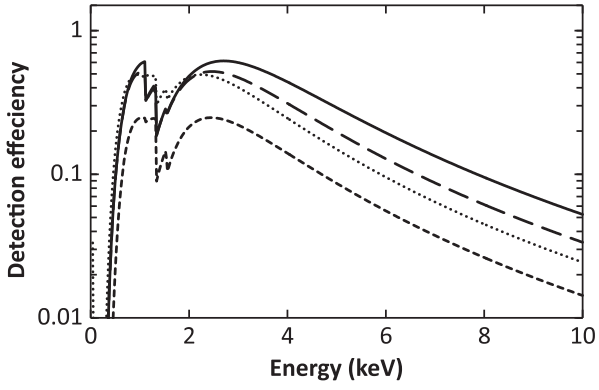

Fig. 3. Calculated detection efficiency as a function of energy for the $Al_{0.2}Ga_{0.8}As$ X-ray p-i-n mesa photodiodes when operated at 30 V (solid line) and 10 V (long dashed line) reverse bias, respectively. For comparison, the detection efficiencies of $Al_{0.8}Ga_{0.2}As$ photodiodes used in Refs. [2,4] are also shown (dotted and short dashed lines respectively). The discontinuities are the Al K, Ga L, and As L X-ray absorption edges.

reported $Al_{0.8}Ga_{0.2}As$ devices [2,4] are also plotted for reference. The detection efficiency (0.134 excluding bondpad attenuation c.f. 0.123 including bondpad attenuation at 5.9 keV) has been calculated under the conservative assumption that the only active region of the detector is the i layer. The greater X-ray linear attenuation coefficients of $Al_{0.2}Ga_{0.8}As$ (e.g. 787.8 cm^{-1} at 5.9 keV) compared with $Al_{0.8}Ga_{0.2}As$ (e.g. 638.8 cm^{-1} at 5.9 keV), together with the thicker i layer for the presently reported detectors, resulted in greater efficiency of the detectors compared with previous photon counting spectroscopic AlGaAs X-ray detectors. The attenuation due to device bondpads has not been included.

3.2. Leakage current

The leakage current as a function of applied reverse bias of each photodiode was measured using a custom dark box and a Keithley 6487 Picoammeter/Voltage Source. National Instruments Labview software was used to automate the characterisation routine. The bias was applied in increments of 0.1 V at a rate of 1 increment per 2 s up to a maximum reverse bias of 30 V. The measurements were made in a dry N_2 environment (< 5% relative humidity) to eliminate any humidity related effects [4]. All three diodes had comparable leakage currents across the measurement range, Fig. 4 presents the leakage current as a function of applied reverse bias for one representative device (D1); the leakage current profile does not represent ideal diode behaviour [17], suggesting that further investigation of the relative contributions of recombination-generation current and diffusion current would be valuable in devices of this type [17,18]. The contributions of these mechanisms could be investigated through temperature dependence of the forward and reverse bias dark currents [18]. At 30 V, the reverse bias at which the detectors were fully depleted, the mean leakage current was 15.4 pA ± 0.4 pA (rms deviance), corresponding to a leakage current density of 49.0 nA cm^{-2} ± 1.3 nA cm^{-2}. Device D2 recorded the lowest leakage current: 15.1 pA ± 0.4 pA, corresponding to 48.0 nA cm^{-2} ± 1.4 nA cm^{-2}.

Recently reported $Al_{0.8}Ga_{0.2}As$ X-ray detectors (400 μm diameter; 1.7 μm i layer) had a leakage current density of 4.72 nA cm^{-2} ± 1.67 nA cm^{-2} at an average electric field strength of 29.4 kV/cm [2]. The presently reported $Al_{0.2}Ga_{0.8}As$ detectors had a larger leakage current density of 9.1 nA cm^{-2} ± 2.1 nA cm^{-2} (a leakage current of 2.8 pA ± 0.7 pA) at the same average electric field strength (equivalent to a reverse bias of 8.8 V for the present detectors). It is also interesting to compare to GaAs mesa photodiodes: recently two 200 μm diameter, 7 μm i layer mesa photodiodes were reported which had leakage current densities of 17.4 nA cm^{-2} and 1.08 nA cm^{-2} respectively, at an average electric field strength of 22 kV/cm [18]. At this field strength (equivalent to an applied reverse bias of 6.6 V for the present devices), the $Al_{0.2}Ga_{0.8}As$ detectors had a mean leakage current density of 7.1 nA cm^{-2} ± 2.7 nA cm^{-2}; device D1 exhibited the lowest leakage current density of the three measured $Al_{0.2}Ga_{0.8}As$ detectors (5.5 nA cm^{-2} ± 1.3 nA cm^{-2}).

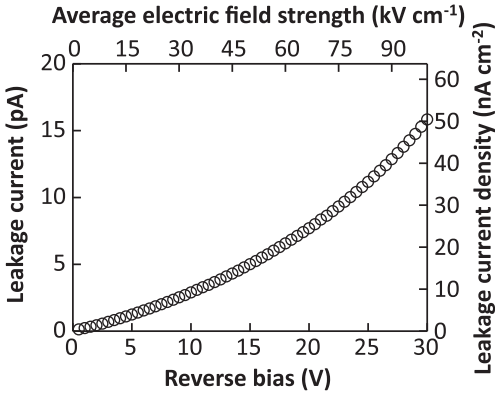

Fig. 4. Measured leakage current for one representative $Al_{0.2}Ga_{0.8}As$ X-ray p-i-n mesa photodiode, D1 in a dry N_2 atmosphere (< 5% relative humidity) as a function of reverse bias. Leakage current density and average electric field strength are also shown for the convenience of the reader.

3.3. X-ray measurements

To investigate the performance of the photodiodes as detectors of soft X-rays, each diode was connected in turn to a custom-made low-noise charge-sensitive single channel preamplifier of feedback resistor-less design similar to Ref. [19]. The preamplifier used a silicon JFET (2N4416A, capacitance = 2 pF) as the input transistor. The preamplifier was connected to an Ortec 571A shaping amplifier (shaping time = 1 μs, the optimum for the system used) and an Ortec 927 ASPEC multi-channel analyser (MCA). An ^{55}Fe radioisotope X-ray source (225 MBq) emitting characteristic Mn Kα (5.9 keV) and Mn Kβ (6.49 keV) X-rays was placed above the AlGaAs diodes. The diodes and preamplifier were operated at room temperature (22 °C) in a dry N_2 environment (< 5% relative humidity). Spectra were accumulated with the photodiodes reverse biased at 0 V, 5 V, 10 V, 15 V, 20 V, and 30 V. The live time limit for each spectrum was 1,000 s. The spectra were energy calibrated using the positions of the zero energy noise peak and the fitted Mn Kα 5.9 keV peak, with the assumption of a linear variation of detected charge with energy. A representative spectrum accumulated with device D1 reverse biased at 10 V is presented in Fig. 5. To minimise counts from the noise peak, a low energy discriminator threshold (3.1 keV) was set. The dashed lines are the Mn Kα and Mn Kβ peaks fitted to the observed peak in the accepted ratio [20], accounting for the relative efficiency of the detector at the respective energies. The FWHM at 5.9 keV measured with D1 under these conditions was 1.3 keV ± 0.1 keV. FWHM at 5.9 keV of 1.2 keV ± 0.1 keV were measured for both D2 and D3. The impact ionization coefficients of $Al_{0.2}Ga_{0.8}As$ as a function of average electric field were calculated and indicated that the diodes were operating within the non-avalanche regime. In addition, no shift in channel number of the Mn Kα 5.9 keV peak as a function of reverse bias was observed.

From Fig. 5, low energy tailing can be seen in the accumulated spectrum. This tailing is attributed to the partial collection of charge created by X-ray photons absorbed in the low-field regions of the photodiode [2]. The valley-to-peak (V/P) ratio can be used to quantify the amount of low energy tailing [2]. For the $Al_{0.2}Ga_{0.8}As$ X-ray p-i-n mesa photodiodes reported, the mean V/P ratio at a reverse bias of 10 V was 0.08. This is comparable to that previously reported for $Al_{0.8}Ga_{0.2}As$ devices [2]. For GaAs (7 μm i layer) at room temperature, an improved V/P ratio (0.05) has been previously shown [18]. As thicker i layer devices are produced, assuming that non-uniformities in the charge collection efficiency, especially at the device edges, are small,

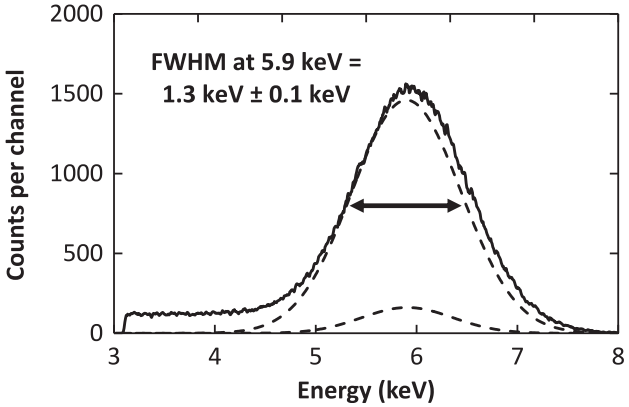

Fig. 5. Spectrum accumulated with $Al_{0.2}Ga_{0.8}As$ device D1 at an applied reverse bias of 10 V when illuminated with an ^{55}Fe radioisotope X-ray source. The dashed lines are the fitted Mn Kα and Mn Kβ peaks.

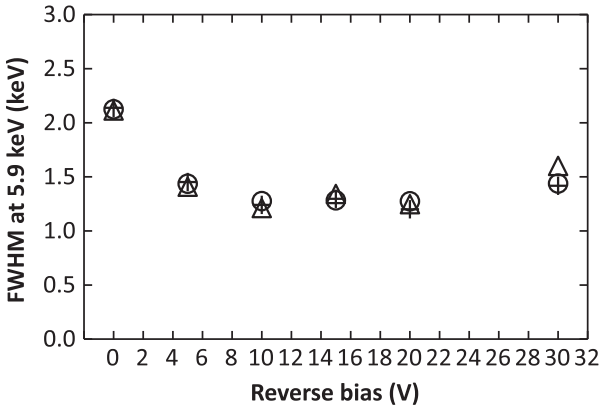

Fig. 6. Measured FWHM at 5.9 keV as a function of applied reverse bias for D1–D3 $Al_{0.2}Ga_{0.8}As$: D1 (circles), D2 (+ symbols) and D3 (triangles).

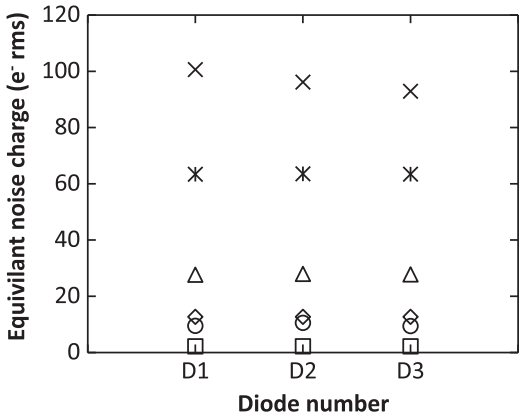

Fig. 7. Calculated remaining noise contributions of each $Al_{0.2}Ga_{0.8}As$ diode at an applied reverse bias of 10 V and a shaping time of 1 μs: combined unknown dielectric noise, incomplete charge collection noise and any additional stray series white noise (crosses); known dielectric noise (stars); series white noise (triangles); Fano noise (diamonds); parallel white noise (circles); $1/f$ series noise (squares).

it is likely that the V/P ratio will improve due to a greater fraction of the X-ray photons illuminating the devices being absorbed in the active region compared with the low-field layers.

The FWHM at 5.9 keV observed with each diode reverse biased at 0 V, 5 V, 10 V, 15 V, 20 V, and 30 V is presented in Fig. 6. The best mean FWHM at 5.9 keV (= 1.24 keV) was observed when the diodes were operated at 10 V and 20 V. An improving trend in FWHM from 0 V to 10 V was attributed to a reduction in capacitance and associated series white noise, in combination with a decrease in charge trapping noise, as discussed in Section 4. Noise Analysis. Between 20 V and 30 V, an increase in FWHM indicated that the leakage current and associated parallel white noise outweighed any positive aspects brought from operation at higher reverse bias.

4. Noise analysis

The fundamental (Fano-limited) energy resolution (ΔE) of a non-avalanche X-ray photodiode is given by,

$$\Delta E = 2.355\omega\sqrt{FE/\omega}, \tag{2}$$

where F is the Fano factor, E is the energy of the photon, and ω is the average energy consumed in the generation of an electron-hole pair [2,21]. The electron hole pair creation energy (ω) can also be expressed in terms of the number of electron hole pairs (n) and the photon energy (E) by,

$$\omega = E/n. \tag{3}$$

Assuming a Fano factor of 0.12, and an electron hole pair creation energy of 4.4 eV (assuming a linear variation of ω with Al fraction between GaAs [22] and $Al_{0.8}Ga_{0.2}As$ [4]), the expected Fano limited energy resolution (FWHM) at 5.9 keV would be 131 eV for $Al_{0.2}Ga_{0.8}As$ at room temperature. However, it is often the case that the energy resolution of a detector is further degraded by electronic noise [2] and noise from the incomplete collection of charge (including charge trapping) [23], such that Eq. (2) becomes,

$$\Delta E = 2.355\omega\sqrt{\left(\frac{FE}{\omega}\right) + a^2 + r^2}, \tag{4}$$

where r is the incomplete charge collection noise in equivalent noise charge (in units of e^- rms) and a is the electronic noise equivalent noise charge (in units of e^- rms). Given that the experimentally observed energy resolutions (FWHM) of the diodes are much greater than the Fano-limit, it is important to consider the relative contributions of the additional noise sources.

Electronic noise contributions include parallel white noise, series white noise, induced gate drain current noise, $1/f$ series noise, and dielectric noise [2]. Fig. 7 presents the calculated values of these noise contributions, as per Refs. [24–26], for each diode when reverse biased at 10 V.

In addition to the parallel white noise of the detector, the parallel white noise contribution from the JFET was also included within the total parallel white noise contribution, assuming that the leakage current of the JFET at room temperature was 1 pA [27]. As the contribution from series white noise depends on the total capacitance load at the gate of the input transistor of the preamplifier, only a minimum estimate could be calculated. This is due to the prototype nature of the preamplifier, where, in addition to estimable capacitances, stray capacitances with unknown values are present. Similarly, dielectric noise contributions arising from the detector, JFET and feedback capacitor were readily estimated [2,8], but additional noise from other lossy dielectrics in proximity to the preamplifier would also have added to the noise. Subtracting the expected Fano noise (the statistically limited resolution) and the electronic noise contributions (parallel white noise, known series white noise (including induced gate drain current noise), known dielectric noise, and $1/f$ noise) from the measured FWHM in quadrature, the remainder can be attributed to incomplete charge collection noise, and the unknown dielectric and stray series white noises [2].

From Fig. 7, the dominant source of noise across all diodes was this remaining noise. Assuming the remaining noise from unknown lossy dielectrics and stray series white noise was independent of reverse bias [24,26], the reduction of this remaining noise as the reverse bias was increased from 0 V to 10 V can be attributed to a reduction in charge trapping noise (the prime constituent of incomplete charge collection noise broadening the energy resolution).

Given this assumption, a quantitative estimate of the reduction of charge trapping noise as a function of increased applied bias can be made by subtracting the known noise contributions that vary with applied reverse bias from the equivalent noise charge of the measured FWHM at each reverse bias in quadrature, and examining the change in the remainder as a function of applied reverse bias [24]. Therefore, it can be said that there was a mean additional charge trapping noise of 146 e^- rms equivalent noise charge (ENC) at 5.9 keV when the detectors were operated at 0 V in comparison to 5 V reverse bias. Similarly, a mean additional charge trapping noise of 67 e^- rms ENC at 5.9 keV was calculated at 5 V in comparison to 10 V. Beyond this reverse bias, any remaining charge trapping noise became insignificant compared with the other noise components. The calculated charge trapping noise was then subtracted from the unknown dielectrics, incomplete charge collection and additional series white noise in quadrature. The various noise components are presented in Fig. 8 for one representative diode (D1). The $Al_{0.8}Ga_{0.2}As$ (400 μm diameter,

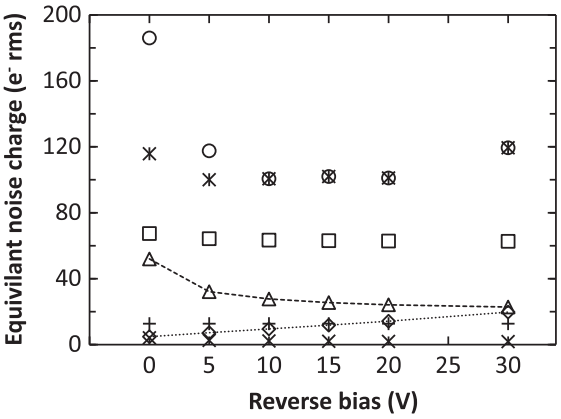

Fig. 8. Calculated remaining noise contributions (unknown dielectric noise, incomplete charge collection noise and additional series white noise) (circles), remaining noise contributions with charge trapping noise subtracted (stars), known dielectric noise (squares), series white noise (triangles), Fano noise (plus signs), parallel white noise (diamonds) and $1/f$ series noise (crosses) as a function of applied reverse bias, at a shaping time of 1 μs, for one representative $Al_{0.2}Ga_{0.8}As$ X-ray p-i-n mesa photodiode, D1, at room temperature. The dashed lines are guides for the eyes only.

1.7 μm i layer) photodiodes reported in Ref. [2], had 26 e^- rms ENC charge trapping noise at 5.9 keV at 5 V reverse bias; significantly less than the presently reported detectors (67 e^- rms ENC at 5 V reverse bias). This is not surprising given the maturity of $Al_{0.8}Ga_{0.2}As$ as a material for X-ray spectroscopy compared with that of $Al_{0.2}Ga_{0.8}As$. Additionally, as can be seen in Fig. 8, an apparent increase in the noise attributed to unknown lossy dielectrics and stray series white noise occurred between 20 V and 30 V reverse bias. One possible explanation for this is that rather than an increase in these particular noise components, there may have been an increase in parallel white noise from the preamplifier's input JFET as a result of the larger leakage current of the detector at 30 V compared with 20 V reverse bias. Such dependence of the JFET's performance was negligible at lower detector leakage currents but could have had a small effect at higher leakage currents due to the bias condition of the JFET being controlled, in part, by the leakage current of the detector in feedback resistorless preamplifiers [19].

5. Conclusions and further work

For the first time, the material $Al_{0.2}Ga_{0.8}As$ has been characterised for soft X-ray spectroscopy via a set of three p-i-n (200 μm diameter, 3 μm i layer) photodiodes. The material has been shown to be suitable for photon counting X-ray spectroscopy at room temperature with the performance of the system primarily limited by the performance of the preamplifier electronics rather than the material's inherent properties. The diodes were fully depleted at an applied reverse bias of 30 V, with a calculated mean depletion width of 3.02 μm ± 0.12 μm across the three diodes and a mean leakage current of 15.4 pA ± 0.4 pA (rms deviance), corresponding to a leakage current density of 49.0 nA cm^{-2} ± 1.3 nA cm^{-2}. At 10 V (leakage current = 3.2 pA ± 0.5 pA) the mean energy resolution was calculated to be 1.24 keV FWHM at 5.9 keV. The measured energy resolutions (FWHM at 5.9 keV) of the $Al_{0.2}Ga_{0.8}As$ diodes are comparable to recent reports using $Al_{0.8}Ga_{0.2}As$, where a mean energy resolution of 1.27 keV ± 0.04 keV FWHM at 5.9 keV was found for 400 μm devices [2]; however, the currently reported energy resolutions achieved with the $Al_{0.2}Ga_{0.8}As$ X-ray photodiodes are modest compared with those recently achieved using state-of-the-art Silicon Drift Detectors (SDDs) coupled to state-of-the-art ultra-low-noise CMOS readout electronics, even at room temperature (FWHM = 141 eV at 5.9 keV [28]). The best reported energy resolution for non-avalanche AlGaAs X-ray detectors (200 μm diameter; 1 μm i layer) is currently 1.07 keV FWHM at 5.9 keV [15].

Data underlying this work are subject to commercially confidentiality. The Authors regret that they cannot grant public requests for further access to any data produced during the study, however the key findings are fully included within the article.

The results indicate that $Al_{0.2}Ga_{0.8}As$ is a potentially promising material for room temperature photon counting X-ray spectroscopy. $Al_{0.2}Ga_{0.8}As$ detectors with thicker i layers than previous $Al_{0.8}Ga_{0.2}As$ photon counting X-ray detectors, and comparable energy resolutions have been demonstrated. Whilst the results are promising, in order to be competitive with GaAs detectors, the detection efficiency (thickness) will have to be increased and the energy resolution improved: GaAs detectors of thicker i layer (e.g. 7 μm [18] and 40 μm [29]) and better energy resolution (745 eV [18] and 266 eV [29]) have been demonstrated. SiC has also been shown to possess excellent energy resolution at room temperature (196 eV FWHM at 5.9 keV [30]), and despite its significantly lower linear attenuation coefficients (e.g. 348.2 cm^{-1} at 5.9 keV [31]) compared to those of AlGaAs (e.g. 787.8 cm^{-1} at 5.9 keV [31] for $Al_{0.2}Ga_{0.8}As$) and GaAs (e.g. 836.7 cm^{-1} at 5.9 keV [31]), SiC is still a highly competitive technology for soft X-ray spectroscopy with the availability of thicker structures offsetting the lower linear attenuation coefficients. Other wide band gap materials such as AlInP and AlInAs could also prove suitable for photon counting X-ray detection. $Al_{0.52}In_{0.48}P$ (2 μm i layer) was recently characterised at room temperature, where an energy resolution of 930 eV FWHM at 5.9 keV was reported [32], whilst maintaining < 3 nA cm^{-2} leakage current densities [32]. $Al_{0.52}In_{0.48}P$ avalanche photodiodes have also been characterised, where an energy resolution of 682 eV FWHM at 5.9 keV has been reported [33]. The increasing research in X-ray detection employing ternary semiconducting structures will undoubtedly yield further materials suitable for replacing Si photon counting X-ray detectors, better equipped to handle intense radiation and high temperature conditions.

In future work, characterisation of $Al_{0.2}Ga_{0.8}As$ detectors of different diameters and thicknesses will be reported, as will characterisation of their response to illumination with X-ray photons of different energy. The temperature dependence of the performance of the devices will also be investigated and measurements of the electron-hole pair creation energy will be reported.

Authors' data statement

Data underlying this work are subject to commercially confidentiality. The Authors regret that they cannot grant public requests for further access to any data produced during the study, however the key findings are fully included within the article.

Acknowledgments

This work was supported by Science and Technology Facilities Council, UK, Grants ST/M002772/1 and ST/M004635/1, and Royal Society, UK, Grant RS130515 (University of Sussex, A.M.B., PI). M.D.C.W. and G.L. each independently acknowledge funding received in the form of Ph.D. scholarships from University of Sussex. The authors are grateful to B. Harrison, R. J. Airey, and S. Kumar at the EPSRC National Centre for III-V Technologies for material growth and fabrication.

References

[1] J. Lauter, et al., Nucl. Instrum. Methods Phys. Res. Sect. A 356 (1995) 324.
[2] A.M. Barnett, G. Lioliou, J.S. Ng, Nucl. Instrum. Methods Phys. Res. Sect. A 774 (2015) 29.
[3] A. Silenas, et al., Nucl. Instrum. Methods Phys. Res. Sect. A 563 (2006) 21.
[4] A.M. Barnett, J.E. Lees, D.J. Bassford, J. Instrum. 8 (2013) P10014.
[5] A. Silenas, et al., Nucl. Instrum. Methods Phys. Res. Sect. A 633 (2011) S62.
[6] S. Adachi, J. Appl. Phys. 58 (1985) R1.
[7] G. Bertuccio, R. Casiraghi, IEEE Trans. Nucl. Sci. 50 (2003) 175.

[8] G. Lioliou, A.M. Barnett, Nucl. Instrum. Methods Phys. Res. Sect. A 801 (2015) 63.
[9] L. Berger, Semiconductor Materials, CRC Press, Boca Raton, 1996.
[10] S.P. Swierkowski, G.A. Armantrout, IEEE Trans. Nucl. Sci. 22 (1975) 205.
[11] G.A. Armantrout, et al., IEEE Trans. Nucl. Sci. 24 (1977) 121.
[12] A.M. Barnett, et al., J. Instrum. 7 (2012) P06016.
[13] A.M. Barnett, J.E. Lees, D.J. Bassford, Appl. Phys. Lett. 102 (2013) 181119.
[14] A. Owens, Compound Semiconductor Radiation Detectors, CRC Press, Boca Raton, 2012.
[15] A.M. Barnett, et al., Nucl. Instrum. Methods Phys. Res. Sect. A 621 (2010) 453.
[16] S. Adachi, Properties of Aluminium Gallium Arsenide, INSPEC, The Institution of Electrical Engineers, London, 1993 [EMIS Datareviews Series No. 7].
[17] S.M. Sze, Physics of Semiconductor Devices, 3rd edition, John Wiley & Sons, New Jersey, 2007.
[18] G. Lioliou, et al., Nucl. Instrum. Methods Phys. Res. Sect. A 813 (2016) 1.
[19] G. Bertuccio, P. Rehak, D. Xi, Nucl. Instrum. Methods Phys. Res. Sect. A 326 (1993) 71.
[20] U. Schötzig, Appl. Radiat. Isot. 53 (2000) 469.
[21] R. Jenkins, Quantitative X-ray Spectrometry, CRC Press, Boca Raton, 1995.
[22] G. Bertuccio, D. Maiocchi, J. Appl. Phys. 92 (2002) 1248.
[23] A. Owens, A. Peacock, Nucl. Instrum. Methods A 531 (2004) 18.
[24] G. Bertuccio, A. Pullia, G. De Geronimo, Nucl. Instrum. Methods Phys. Res. Sect. A 380 (1996) 301.
[25] E. Gatti, et al., Nucl. Instrum. Methods Phys. Res. Sect. A 297 (1990) 467.
[26] A.M. Barnett, et al., Nucl. Instrum. Methods Phys. Res. Sect. A 673 (2012) 10.
[27] Siliconix, 1997, 2N4416/2N4416A/SST4416 N-Channel JFETs, Data Sheet, S-52424, Rev. E, 14-Apr-97, Vishay Electronic GmbH, Selb, Germany.
[28] G. Bertuccio, et al., J. Instrum. 10 (2015) P01002.
[29] A. Owens, et al., J. Appl. Phys. 90 (2001) 5376.
[30] G. Bertuccio, et al., Nucl. Instrum. Methods Phys. Res. Sect. A 652 (2011) 193.
[31] D.T. Cromer, D. Liberman, J. Chem. Phys. 53 (1970) 1891.
[32] S. Butera, G. Lioliou, A.B. Krysa, A.M. Barnett, J. Appl. Phys. 120 (2016) 024502.
[33] A. Auckloo, J.S. Cheong, X. Meng, C.H. Tan, J.S. Ng, A. Krysa, R.C. Tozer, J.P.R. David, J. Instrum. 11 (2016) P03021.